Subtropical High predictability establishes a promising way for monsoon and tropical storm predictions

Bin Wang[a,b,1], Baoqiang Xiang[b], and June-Yi Lee[b]

[a]Department of Meteorology, and [b]International Pacific Research Center, University of Hawaii at Manoa, Honolulu, HI 96822

Edited by John M. Wallace, University of Washington, Seattle, WA, and approved December 12, 2012 (received for review August 22, 2012)

Monsoon rainfall and tropical storms (TSs) impose great impacts on society, yet their seasonal predictions are far from successful. The western Pacific Subtropical High (WPSH) is a prime circulation system affecting East Asian summer monsoon (EASM) and western North Pacific TS activities, but the sources of its variability and predictability have not been established. Here we show that the WPSH variation faithfully represents fluctuations of EASM strength ($r = –0.92$), the total TS days over the subtropical western North Pacific ($r = –0.81$), and the total number of TSs impacting East Asian coasts ($r = –0.76$) during 1979–2009. Our numerical experiment results establish that the WPSH variation is primarily controlled by central Pacific cooling/warming and a positive atmosphere-ocean feedback between the WPSH and the Indo-Pacific warm pool oceans. With a physically based empirical model and the state-of-the-art dynamical models, we demonstrate that the WPSH is highly predictable; this predictability creates a promising way for prediction of monsoon and TS. The predictions using the WPSH predictability not only yields substantially improved skills in prediction of the EASM rainfall, but also enables skillful prediction of the TS activities that the current dynamical models fail. Our findings reveal that positive WPSH–ocean interaction can provide a source of climate predictability and highlight the importance of subtropical dynamics in understanding monsoon and TS predictability.

Summer monsoons and tropical storms (TSs) affect billions of people's livelihoods over East Asia including China, Japan, Korea, Indo-China peninsula, and Philippines. Prediction of the East Asian summer monsoon (EASM) rainfall and the TS in the western North Pacific (WNP) is a forefront scientific challenge of great societal importance and economic value. The latest assessment of the world-class climate models' performance clearly demonstrates the models' poor skills in prediction of the monsoon rainfall (1) and their inability to predict WNP TS variations.

The western Pacific Subtropical High (WPSH) has profound effects on (and interact with) EASM and WNP TS activities (2–6); it also has far reaching influence on the summer rainfall over the Great Plains of the United States through atmospheric teleconnection (7, 8). Understanding the mechanism and predictability of the WPSH is a prerequisite for better prediction of the EASM and WNP TS.

It has been noticed decades ago that an enhanced WPSH occurs during El Niño decaying summer, but the physical interpretation was not offered until the turn of 21st century (9–11). Recently, the influence of the Indian Ocean (IO) warming (12) has been revived to explain why the WPSH is abnormally strong after a peak El Niño (13–17). Note, however, approximately one-half of the strong anomalous WPSH years do not concur with decaying El Niño (Fig. S1) or IO warming (Fig. S2). Thus, it is necessary to reshape the conventional thinking on the causes of the interannual variation of the WPSH.

Here, we reveal two fundamental mechanisms controlling the year-to-year variability of the WPSH, and demonstrate the high predictability of the WPSH, which paves a promising way to predict the monsoon and TS activities.

WPSH Index Indicative of the EASM and WNP TS Variability

Although the general connection between the WPSH and EASM/WNP TS has been recognized for decades, quantitative relationships between them have not firmly established. This problem is in part due to the fact that a variety of interrelated WPSH indices (18–20) and EASM indices (21) has been used to depict their respective variations, which makes it extremely difficult to ascertain a clear qualitative linkage between them. To make progress, here we propose to measure the intensity of WPSH by a single objective index defined by boreal summer (June-July-August; JJA) mean 850 hPa geopotential height (H850) anomaly averaged over the maximum interannual variability center (15°N–25°N, 115°E–150°E) (Fig. S3*A*). The EASM intensity can be objectively measured by the leading principal component of the EASM system (21). Fig. 1*A* shows that the WPSH index is highly indicative of the EASM intensity with a correlation coefficient (r) of –0.92 for the period 1979–2009. Further, the variability of the WPSH highly reflects the variations in the TS genesis and movement (Fig. 1 *B* and *C*). An enhanced WPSH signifies reduced TS days in the subtropical WNP with $r = –0.81$ and decreased numbers of TSs that impact East Asian (Japan, Korea, and East China) coastal areas with $r = –0.76$ (Fig. S3*B*). Compared with the previously used indices (18–20), the WPSH index defined here has a higher correlation with the EASM and WNP TS activities (Table S1). In sum, understanding the sources of WPSH variability and predictability may pave an alternative way for prediction of monsoon and TS activities.

Mechanisms of the Interannual Variability of the WPSH

Note that the year-to-year pulse of the WPSH intensity as measured by the WPSH index is not concurrently correlated with El Niño/Southern Oscillation (ENSO) during boreal summer (Fig. S4*A*; $r = –0.12$ for the period 1979–2009). To unravel the origins of the WPSH fluctuation, we turn to investigate the leading modes of summer mean H850 variation because the first two empirical orthogonal function (EOF) modes of H850 account for 53% (31.0% for EOF-1 and 22.2% for EOF-2) of the total variance over the entire Asian monsoon domain and 74% of the total variance in the WNP region (10°N–30°N, 100°E–180°E). Both principal component (PC)-1 and PC-2 of H850 are significantly correlated with the WPSH index ($r = 0.60$ and $r = 0.73$). Surprisingly, the year-to-year fluctuation of the WPSH intensity can be reconstructed extremely well with the PCs associated with the two EOFs based on the multivariate regression method: (1.289×PC-1 + 1.099×PC-2), and the correlation coefficient between the observed and reconstructed WPSH indices is 0.93 (Fig. S4*D*). Hence, understanding the underlying dynamics of the two EOF modes is of central importance for mining the source of predictability of the WPSH.

Author contributions: B.W. and B.X. designed research; B.W. and B.X. performed research; B.X. and J.-Y.L. analyzed data; and B.W., B.X., and J.-Y.L. wrote the paper.

The authors declare no conflict of interest.

This article is a PNAS Direct Submission.

[1]To whom correspondence should be addressed. E-mail: wangbin@hawaii.edu.

This article contains supporting information online at www.pnas.org/lookup/suppl/doi:10.1073/pnas.1214626110/-/DCSupplemental.

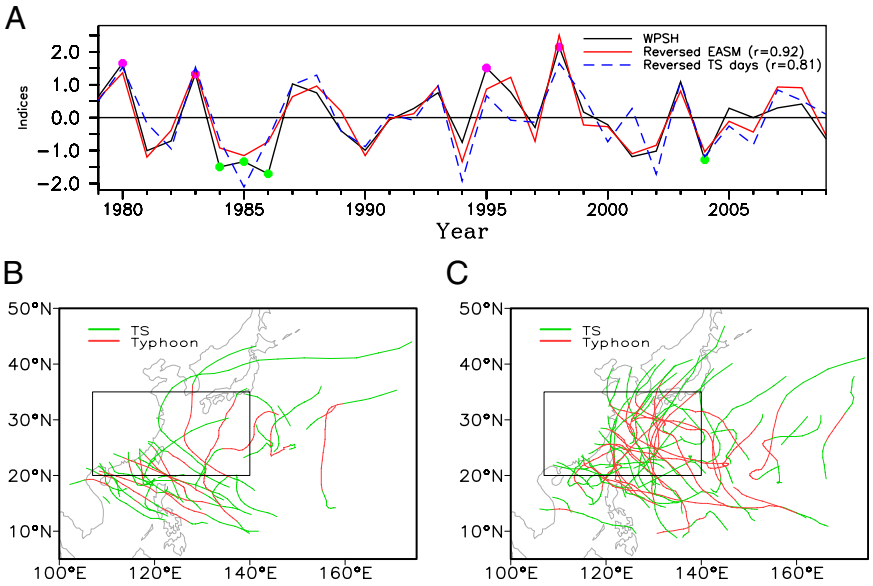

Fig. 1. WPSH and its relationship with EASM intensity and TS activities. (*A*) Interannual variations of the boreal summer (JJA) WPSH intensity index, EASM strength (reversed) and the total number of TS days (reversed) over the subtropical WNP (black boxes in *B* and *C*). The numbers in parentheses indicate correlation coefficients with the WPSH index. (*B*) TS tracks for the four extremely strong WPSH years. *C* is as in *B* but for the four extremely weak WPSH years. The extreme WPSH years with its anomaly above 120% of its standard deviation (SD) are indicated in *A* by the purple (green) dots. The green lines represent the TS with maximum wind speed above 17.5 m/s but less 32.5 m/s, and the red lines represent typhoon with maximum wind speed above 33 m/s.

The EOF-1 is characterized by an intense southwest-northeast–oriented WPSH, which concurs with suppressed rainfall on its southeast flank and enhanced rainfall in Korea, Japan, and the equatorial Pacific (Fig. 2*A*). How can this WPSH anomaly sustain itself given the chaotic nature of the atmospheric motion? We argue that a positive feedback between the WPSH and underlying dipolar sea surface temperature (SST) anomaly in the Indo-Pacific warm pool (Fig. 2*B*) plays a central role. First, to the southeast of the WPSH anomaly, the SST is cool because the anomalous northeasterly winds strengthen mean easterlies to the east of the monsoon trough, thereby enhancing evaporation/entrainment (Fig. S5). Conversely, the resultant ocean cooling would, in turn, reduce in situ precipitation heating (Fig. 2*A*), hence generating descending Rossby waves that reinforce the WPSH in their westward decaying journey (9). This positive thermodynamic feedback is confirmed by numerical experiments with a coupled model (22) (Fig. S6), which demonstrates that an initial SST cooling in the WNP can indeed maintain an anomalous WPSH in the ensuing summer (Fig. 2*C*). Second, to the southwest of the enhanced WPSH, the northern IO warms because the easterly anomalies associated with the WPSH weaken the southwest monsoons (Fig. 2*B*), thereby reducing surface latent heat flux (23). Conversely, the northern IO warming would help sustain the WPSH (refs. 13–17; Fig. S7). Thus, the interplay between the WPSH and northern IO warming also contributes to the maintenance of the WPSH. In sum, the EOF-1 can be viewed as an atmosphere–ocean interaction mode and the mechanism for the EOF-1 is summarized in Fig. S7.

The EOF-2 mode features a strong anomalous WPSH and a weak IO low (Fig. 3*A*). The anomalous WPSH ridge and the associated suppressed convection extend from the Philippine Sea southeastward to the equatorial western Pacific. The enhanced WPSH concurs with equatorial central Pacific cooling (Fig. 3*B*); the corresponding principal component is negatively correlated with the Niño3.4 index [SST anomaly (SSTA) averaged over 5°S–5°N, 170°W–120°W (r = –0.68), Fig. S4*C*]. It suggests that the EOF-2 mode reflects a developing (or persisting) La Niña event signifying a stronger than normal WPSH, and vice versa. The enhanced WPSH associated with the EOF-2 is arguably forced by the central Pacific cooling that shifts the east-west circulation (Walker) cell with the rising limb shifting westward, thus reducing convection around 160°E and increasing convection over the maritime continent (Fig. 3*A*). The suppressed convection can directly strengthen the WPSH by emanation of descending Rossby waves. This assertion is confirmed by numerical experiments with the ECHAM atmospheric general circulation model (24) forced by the central Pacific SST cooling, which reproduces realistic precipitation and H850 anomalies (Fig. 3*C*). Meanwhile, the reinforced maritime continent convection can also enhance the WPSH via inducing equatorial easterlies over the western Pacific (25), which generates off-equatorial anticyclonic shear vorticity over the Philippine Sea.

High Predictability of the WPSH

To estimate the lower bound of the predictability for the WPSH, we built an empirical model to predict the WPSH intensity with three predictors based on multivariate regression that are tightly linked to the first two EOF modes (Fig. S8):

$$\text{WPSH index} = 1.704 \times \text{SSTA(IO} - \text{WNP)} - 0.713 \times \text{ENSO}_{\text{develop}} - 0.283 \times \text{NAOI}, \quad [1]$$

where SSTA(IO-WNP) represents the April–May mean dipolar SSTA difference between the IO (10°S–10°N, 50°E–110°E) and the WNP (0°–15°N, 120°E–160°E), which acts as a predictor for the EOF-1 (r = 0.76). The $\text{ENSO}_{\text{develop}}$ denotes the May-minus-March SSTA in the central Pacific (15°S–5°N, 170°W–130°W), which is a predictor for the EOF-2 (r = –0.47). Additionally, the North Atlantic Oscillation (NAO) (26) index (NAOI) in April–May is used as a predictor for EOF-2 (r = –0.38), because the NAOI (27) was found to be a complementary predictor for EASM (28, 29). Physically, the SSTA associated with anomalous NAO in April–May can lead to the equatorial Pacific SSTA during the following summer (29) (Fig. S8*C*), thus providing a predictor for the EOF-2. Hence, all three predictors are selected based on the physical processes that govern the two predictable EOF modes.

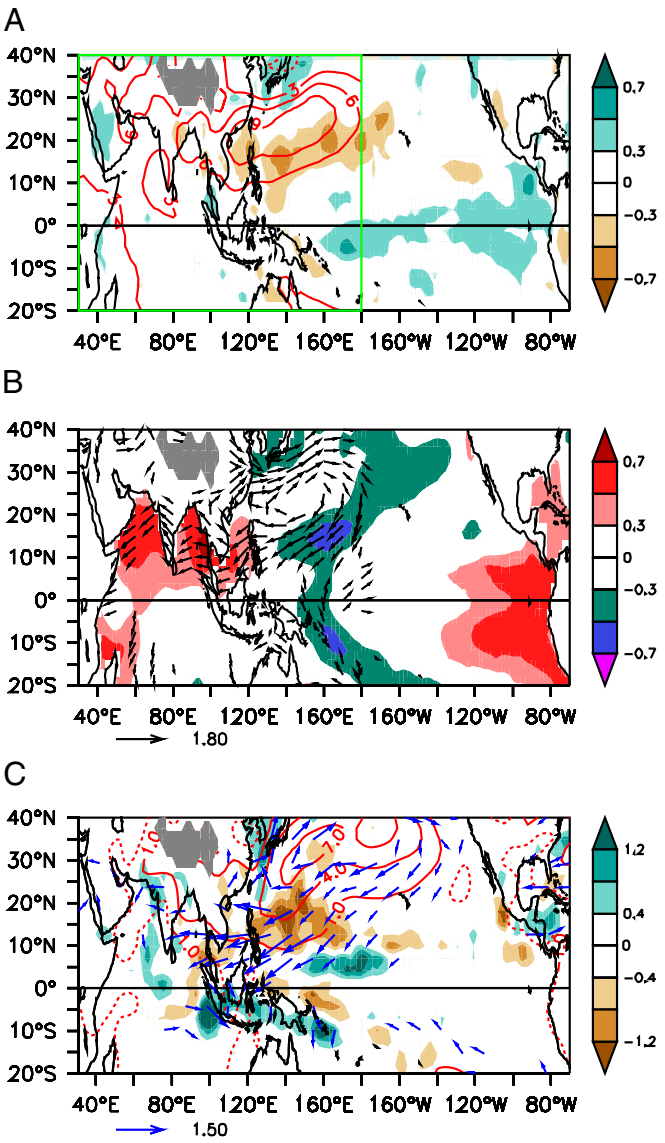

Fig. 2. Origins of the EOF-1 (the coupled atmosphere-ocean) mode. (*A*) Spatial pattern (contours) of the leading EOF mode derived from summer (JJA) H850 in the Asian-Australian monsoon domain (20°S–40°N, 30°E–180°E). Shown is also the correlated precipitation (shading) in the Indo-Pacific domain with correlations significant at 90% confidence ($r > 0.3$). (*B*) The correlated SSTA (shading) and 850 hPa wind anomalies with reference to the PC of EOF-1. (*C*) The simulated JJA mean precipitation (shading in millimeters per day), H850 (contours in meters) and 1,000 hPa wind anomaly (only vectors with absolute value larger than 0.3 m/s are shown) in response to an initial SST perturbation over the WNP in a coupled model experiment (Fig. S6).

The physically based prediction model (Eq. **1**) can reproduce the WPSH index realistically with a temporal correlation skill of 0.81 for 1979–2009 (Fig. 4*A*). To test its predictive capability, the cross-validation method (30) with a leaving-three-out approach (31) was used to reforecast the WPSH index. The temporal correlation skill for the 31-y cross-validated reforecast skill is 0.75. As a comparison, we have assessed reforecast performance of three state-of-the-art coupled climate models (32) in predicting the WPSH index with initial conditions on June 1 of each year (Fig. S9*A*). The skills of these dynamical models range from 0.72 to 0.76 with a three-model ensemble mean skill of 0.82 for the period of 1981–2009 (Fig. S9*A*). The high predictability of the WPSH may open a pathway to ameliorate monsoon and TS predictions because of their close relationships with the WPSH (Fig. 1*A*).

Prediction of the EASM and WNP TS

Using WPSH predictors and predictability, we have attempted to directly predict the EASM intensity, the subtropical WNP TS days, and the total number of TSs impacting East Asia; the results show promising and valuable deterministic and probabilistic prediction skills (Fig. 4). The high predictability of the WPSH makes WNP TS prediction possible although the global models generally cannot directly resolve and predict the tropical cyclones. For example, predictions of the subtropical WNP TS days and the total number of TSs impacting East Asian coasts can achieve temporal correlation skills of 0.73 and 0.66, respectively (Fig. 4 *C* and *D*). Furthermore, using the predictability of the two major modes of the WPSH, an empirical model for direct prediction of the EASM rainfall anomalies can be constructed. The direct empirical prediction can provide a significantly higher reforecast skill

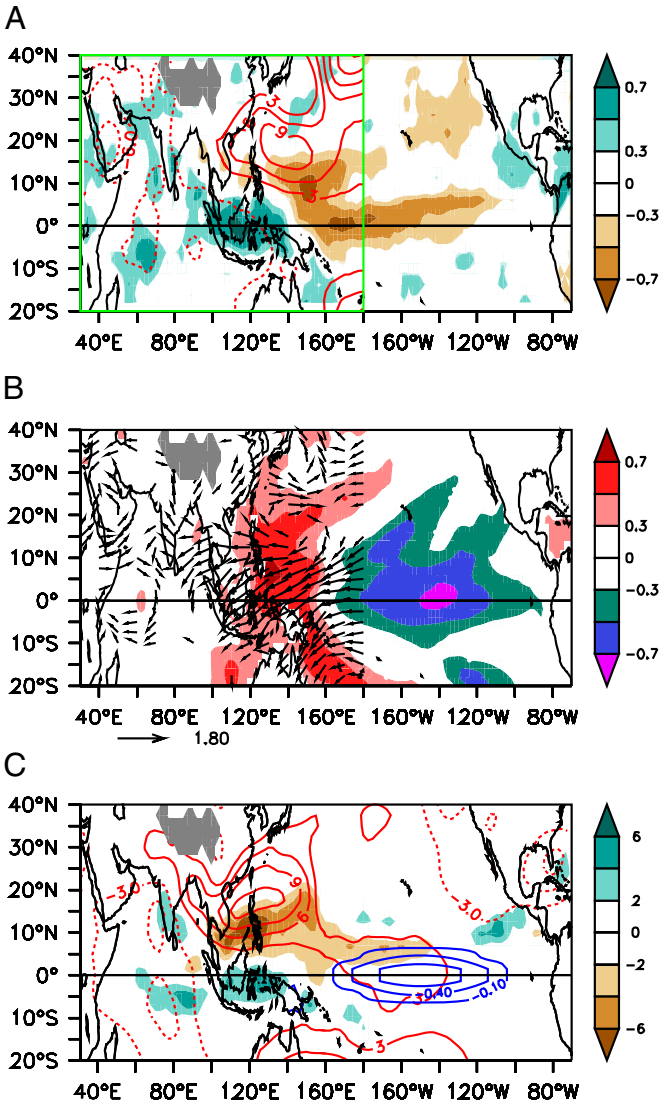

Fig. 3. Origin of the EOF-2 (the forced) mode. (*A* and *B*) The same as in Fig. 2 *A* and *B*, but for the EOF-2 mode. (*C*) Simulated JJA H850 (contours in meters) and precipitation (shading in millimeters per day) anomalies using ECHAM model forced by the prescribed cold SSTA over the equatorial central Pacific (blue contours in Celsius).

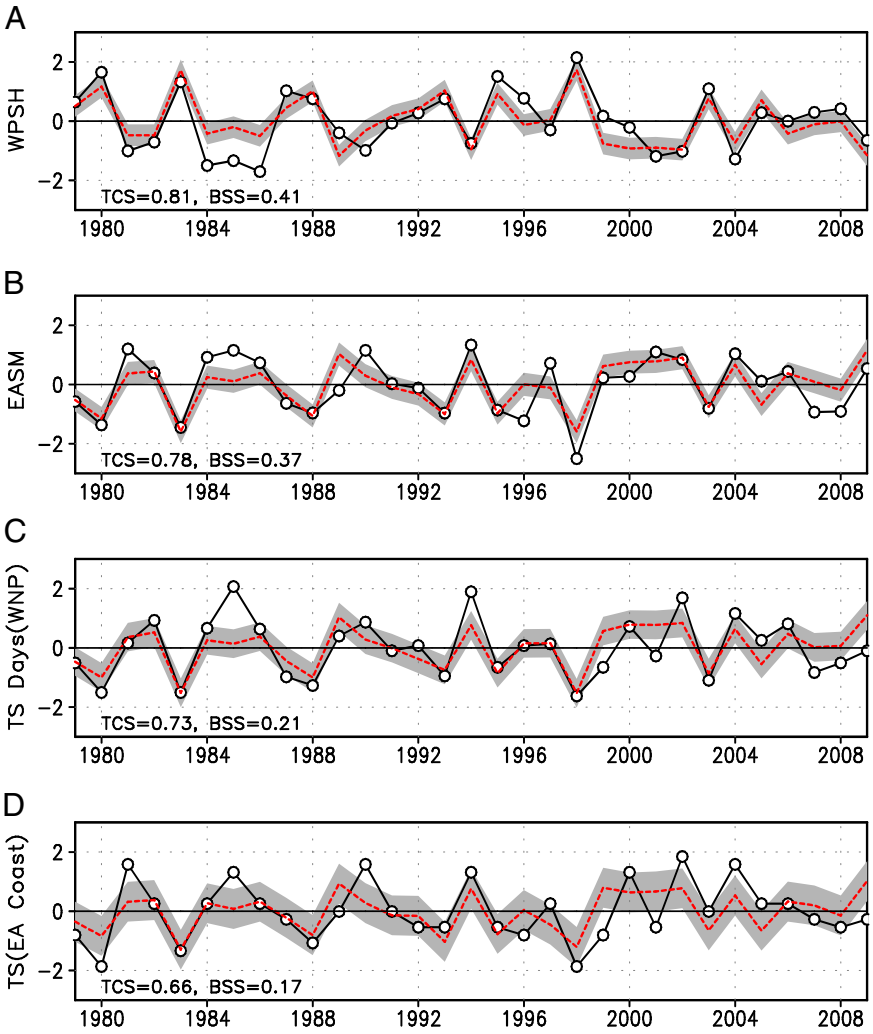

Fig. 4. Prediction of the WPSH, EASM, and WNP TS activities with the physically based empirical models by using WPSH predictability. The observation (black) and prediction (red) of the WPSH index (*A*); the EASM strength (*B*); the TS days over the subtropical WNP (*C*); and the total TS numbers impacting the EA coast regions during JJA (*D*). Uncertainty of the each prediction measured by standard forecast error is given (shading). The deterministic prediction skills in terms of temporal correlation skill (TCS) for these three indices reach 0.81, 0.78, 0.73, and 0.66, respectively, and the corresponding cross-validated reforecast skills reach 0.75, 0.72, 0.68, and 0.59, respectively. The probabilistic prediction skills in terms of Brier skill score (BSS) (1) for the four predictands in *A*–*D* are 0.41, 0.37, 0.21, and 0.17, respectively.

for summer monsoon rainfall than the dynamical models (Fig. S9 *B* and *C*). The temporal correlation skill for prediction of area-averaged rainfall over East Asia (5°N–40°N, 110°E–140°E) is 0.50 (empirical) versus 0.21 (dynamical). Thus, the two mechanisms underlying the WPSH variability provide a physical basis for predicting EASM and the WNP TS, and use of the WPSH predictability can significantly improve the monsoon rainfall and TS predictions.

Discussion

We used observational analyses and numerical experiments to show the fundamental dynamics governing the WPSH variability. Compared with relative mature midlatitude dynamics (quasi-geostrophic theory) and equatorial dynamics (equatorial wave theory), the subtropical dynamics is an area calling for further major efforts to develop our theoretical understanding. We hope that our work paves a way toward developing subtropical dynamics theories.

Traditional theory suggested that climate predictability arises from the forcing in slowly varying lower boundary conditions, such as SST (33, 34). The findings here demonstrate that the WPSH is not just a passive response to SST change, and the positive WPSH–ocean interaction can provide a source of climate predictability that extends ENSO impacts to upstream midlatitudes and to the ENSO transition phases when ENSO forcing is weak or absent. This result adds a perspective to the existing climate predictability theories and for mining sources of the predictability. Our finding also highlights the importance of translating the models' circulation predictability into rainfall and TS predictability and motivates additional research in how changes in subtropical circulation may be influencing long-term trends and future changes of monsoon precipitation and TS impacts.

Methods

Models and Experiments. Two numerical climate models were adopted in this study. The first is an atmospheric general circulation model ECHAM (v4.6) (24). Two sets of forced experiments were carried out by using ECHAM model. One is a control run (20-y) forced with observed climatological SST and sea ice, and the other is a sensitivity experiment (20 ensemble members) with imposed cold SSTA during JJA over the equatorial central Pacific to test whether the EOF-2 mode is a forced mode (Fig. 3*C*). The second model is a coupled model, POEM, which consists of ECHAM (v4.6) atmospheric model and POP (v2.0) ocean model (22). This coupled model reproduces realistic surface wind fields, which provides precondition to testify the positive

thermodynamic feedback in sustaining the WPSH associated with EOF-1 mode (Fig. S6). We conducted two sets of experiments. The first is a control run that is freely coupled (20 y) to provide 20 ensembles of summer climatology. The other is a sensitivity experiment that shares the same initial condition of the above 20 ensemble runs but with an imposed cold SST tendency perturbation in the WNP for 10 d from May 21 to May 31 (Fig. S6*A*). After May 31, the model is relaxed to a free coupled run. We then compared the ensemble mean results averaged in JJA with the control runs to identify whether the initial SSTA can maintain and generate the WPSH anomaly.

Datasets. Several datasets were used in this study, including (*i*) monthly mean SST from National Oceanic and Atmospheric Administration Extended Reconstructed SST (ERSST, v3b) (35); (*ii*) monthly mean precipitation from Global Precipitation Climatology Project (v2.1) datasets (36); and (*iii*) monthly mean circulation data from National Centers for Environmental Prediction–Department of Energy Reanalysis 2 products (37). Summer (JJA) anomalies are calculated by the deviation of JJA mean from the 31-y climatology (1979–2009). We also used the International Best Track Archive for Climate Stewardship (IBTrACS, v03r03) World Meteorological Organization (WMO) data (www.ncdc.noaa.gov/oa/ibtracs/index.php?name=ibtracs-data) to estimate the positions of the TS. The IBTrACS data for TS positions are first transformed into an area-averaged TS frequency at 5×5 degree point. The TS days were then defined as the averaged TS occurrence divided by four because the IBTrACS data for TS positions are reported every 6 h.

EASM Intensity Index. The EASM index used here is based on the first leading multivariate EOF analysis of a set of six JJA mean meteorological fields over the domain (0°–50°N, 100°E–140°E), including precipitation, zonal and meridional winds at 850 hPa and 200 hPa, and sea level pressure (21). This EASM index can capture approximately 38% of the total variance of the precipitation and 3D circulation and has unique advantages over the existing indices (21).

NAOI. The NAOI used in this study is defined by the difference of the normalized sea level pressure anomaly (zonal averaged from 80°W to 30°E) between 35°N and 65°N over the North Atlantic sector (27).

Cross-Validation Method. The cross-validation method (30) is used to make a reforecast of these indices by using the three WPSH predictors. The cross-validation method systematically leaves 3 y out from the period 1979–2009, derives a forecast model by using data of the remaining years, and validates it against unused cases. The predictions in Fig. 4 were made by empirical models by using the same three predictors for the WPSH index.

ACKNOWLEDGMENTS. We thank Shibin Xu and Yuxing Yang for help with TC data and Dr. Tim Li for commenting on an initial version of the manuscript. The revision of the manuscript benefits from comments made by three anonymous reviewers. We acknowledge support of this work from Korean Ministry of Education, Science and Technology Grant 2011-0021927 through Global Research Laboratory Program, National Science Foundation Award AGS-1005599, an Asia-Pacific Economic Cooperation Climate Center (APCC) international project, and International Pacific Research Center that is, in part, supported by Japan Agency for Marine-Earth Science and Technology, National Oceanic and Atmospheric Administration, and National Aeronautics and Space Administration. The International Pacific Research Center (IPRC) publication number is 940 and the School of Ocean and Earth Science and Technology (SOEST) publication number is 8817.

1. Wang B, et al. (2009) Advance and prospect of seasonal prediction: Assessment of APCC/CliPAS 14-model ensemble retrospective seasonal prediction (1980-2004). *Clim Dyn* 33(1):93–117.
2. Miyasaka T, Nakamura H (2005) Structure and formation mechanisms of the Northern Hemisphere summertime subtropical highs. *J Clim* 18(8):5046–5065.
3. Ho C-H, Baik J-J, Kim J-H, Gong D-Y, Sui C-H (2004) Interdecadal changes in summertime typhoon tracks. *J Clim* 17(9):1767–1776.
4. Liu Y, Wu G (2004) Progress in the study on the formation of the summertime subtropical anticyclone. *Adv Atmos Sci* 21(3):322–342.
5. Zhou T-J, Yu R-C (2005) Atmospheric water vapor transport associated with typical anomalous summer rainfall patterns in China. *J Geophys Res* 110:D08104, 10.1029/2004JD005413.
6. Zhou T, et al. (2009) Why the Western Pacific Subtropical High has extended westward since the late 1970s. *J Clim* 22(8):2199–2215.
7. Wang B, Wu R, Lau KM (2001) Interannual variability of Asian summer monsoon: Contrast between the Indian and western North Pacific-East Asian monsoons. *J Clim* 14(20):4073–4090.
8. Lau KM, Weng H (2002) Recurrent teleconnection patterns linking summertime precipitation variability over East Asia and North America. *J Meteorol Soc Jpn* 80(6):1309–1324.
9. Wang B, Wu R, Fu X (2000) Pacific-East Asia teleconnection: How does ENSO affect East Asian climate? *J Clim* 13(9):1517–1536.
10. Chang CP, Zhang Y, Li T (2000) Interannual and interdecadal variation of East Asian summer monsoon and the tropical Pacific SSTs. Part I: Roles of the subtropical ridge. *J Clim* 13(24):4310–4325.
11. Lau N-C, Wang B (2006) *The Asian Monsoon*, ed Wang B (Springer, Heidelberg), pp 479–512.
12. Wu G, Liu H (1995) Neighbourhood response of rainfall to tropical sea surface temperature anomalies part I: Numerical experiment. *Scientia Atmospherica Sinica* 19(4):422–434.
13. Yang J, Liu Q, Xie S-P, Liu Z, Wu L (2007) Impact of the Indian Ocean SST basin mode on the Asian summer monsoon. *Geophys Res Lett* 34:L02708.
14. Wu B, Zhou T, Li T (2009) Seasonally evolving dominant interannual variability modes of East Asian climate. *J Clim* 22(11):2992–3005.
15. Xie S-P, et al. (2009) Indian Ocean capacitor effect on Indo-western Pacific climate during the summer following El Niño. *J Clim* 22(3):730–747.
16. Chowdary JS, et al. (2010) Predictability of summer Northwest Pacific climate in 11 coupled model hindcasts: Local and remote forcing. *J Geophys Res-Atmos* 115:D22121.
17. Wu B, Li T, Zhou T (2010) Relative contributions of the Indian Ocean and local SST anomalies to the maintenance of the Western North Pacific anomalous anticyclone during the El Nino decaying summer. *J Clim* 23(11):2974–2986.
18. Chen G (1999) *The Subtropical High. The Droughts and Floods in Summer in China and Background Fields*, ed Zhao Z (China Meteorol Press, Beijing), pp 45–52, Chinese.
19. Sui C-H, Chung P-H, Li T (2007) Interannual and interdecadal variability of the summertime western North Pacific subtropical high. *Geophys Res Lett* 34:L11701, 10.1029/2006GL029204.
20. Wu B, Zhou T (2008) Oceanic origin of the interannual and interdecadal variability of the summertime western Pacific subtropical high. *Geophys Res Lett* 35:L13701.
21. Wang B, et al. (2008) How to measure the strength of the East Asian summer monsoon. *J Clim* 21(17):4449–4461.
22. Xiang B, et al. (2012) Reduction of the thermocline feedback associated with mean SST bias in ENSO simulation. *Clim Dyn* 39(6):1413–1430, 10.1007/s00382-011-1164-4.
23. Du Y, Xie S-P, Huang G, Hu K (2009) Role of air-sea interaction in the long persistence of El Niño-induced North Indian Ocean warming. *J Clim* 22(8):2023–2038.
24. Roeckner E, et al. (1996) The atmospheric general circulation model ECHAM-4: Model description and simulation of present-day climate. *Max-Planck-Institute for Meteorology Rep.* 218:90.
25. Chung PH, Sui C-H, Li T (2011) Interannual relationships between the tropical sea surface temperature and summertime subtropical anticyclone over the western North Pacific. *J Geophys Res* 116:D13111.
26. Ambaum MHP, Hoskins BJ, Stephenson DB (2001) Arctic Oscillation or North Atlantic Oscillation? *J Clim* 14(16):3495–3507.
27. Li J, Wang J (2003) A new North Atlantic Oscillation index and its variability. *Adv Atmos Sci* 20(5):661–676.
28. Wu Z, Wang B, Li J, Jin F-F (2009) An empirical seasonal prediction model of the East Asian summer monsoon using ENSO and NAO. *J Geophys Res* 114:D18120.
29. Gong D-Y, et al. (2011) Spring Arctic Oscillation-East Asian summer monsoon connection through circulation changes over the western North Pacific. *Clim Dyn* 37(11–12):2199–2216, 10.1007/s00382-011-1041-1.
30. Michaelsen J (1987) Cross-validation in statistical climate forecast model. *J Clim Appl Meteorol* 26(11):1589–1600.
31. Blockeel H, Struyf J (2002) Efficient algorithms for decision tree cross- validation. *J Mach Learn Res* 3:621–650.
32. Lee J-Y, et al. (2011) How predictable is the Northern Hemisphere summer upper-tropospheric circulation? *Clim Dyn* 37(5–6):1189–1203.
33. Charney JG, Shukla J (1981) in *Monsoon Dynamics,* eds Sir Lighthill J, Pearce RP (Cambridge Univ Press, London) pp 99–109.
34. Shukla J (1998) Predictability in the midst of chaos: A scientific basis for climate forecasting. *Science* 282(5389):728–731.
35. Smith TM, Reynolds RW, Peterson TC, Lawrimore J (2008) Improvements to NOAA's historical merged land-ocean surface temperature analysis (1880-2006). *J Clim* 21(10):2283–2293.
36. Huffman GJ, Adler RF, Bolvin DT, Gu G (2009) Improving the global precipitation record: GPCP Version 2.1. *Geophys Res Lett* 36:L17808.
37. Kanamitsu M, et al. (2002) NCEP-DOE AMIP-II Reanalysis (R-2). *Bull Am Meteorol Soc* 83(11):1631–1643.